OPEN ACCESS

Laser-triggered lightning discharge

New Journal of Physics
An Institute of Physics and Deutsche Physikalische Gesellschaft Journal

Laser-triggered lightning discharge

Nasrullah Khan, Norman Mariun, Ishak Aris and J Yeak
Department of Electrical and Electronic Engineering, Faculty of Engineering, University Putra Malaysia, 43400 Serdang, Selangor, Malaysia
E-mail: khan@eng.upm.edu.my

New Journal of Physics **4** (2002) 61.1–61.20 (http://www.njp.org/)
Received 24 June 2002
Published 15 August 2002

Abstract. Advances in ultrafast optics in recent years have revived a keen interest in laser-induced dielectric breakdown study. While it is widely accepted that femtosecond laser pulses with peak powers reaching gigawatts can propagate over tens of metres under laboratory conditions, the dynamics underlying this highly nonlinear phenomenon is yet not fully understood. Although initial research on laser-triggered lightning was started with infrared lasers, it was found that they are not suitable to initiate lightning. Recent published literature and experimental work favour the use of ultraviolet (UV) laser pulses as the appropriate means for laser-induced lightning discharge. An analytical solution based on Maxwell's equations has been developed for UV filamentation in air, arising from a dynamic oscillating balance between self-focusing, diffraction and plasma defocusing. This model suggests that UV (220–420 nm) 200 ps laser pulses with a peak power of around 50 MW (or 12.5 mJ input energy) and a beam size of 100 μm are the optimal tool to trigger outdoor lightning. The laser beam size remains relatively small (less than 0.3 mm) after a propagation distance of 200 m up into the normally cloudy and damp atmospheric conditions.

1. Introduction

Since time immemorial, mankind has always beheld lightning with great awe. This is mainly due to the destructive damage caused by lightning strikes. The countless deaths and injuries to livestock, thousands of forest bush fires as well as untold millions of dollars in damage to buildings, communications systems, power lines and electrical systems are mainly the direct result of lightning [1]. In Malaysia, the eastern Malaysian power grid system was struck by lightning that crippled power stations across the nation, bringing the total damage and cost to an estimated RM200 million loss [2]! Aircraft and space shuttles are also not immune to lightning strikes. In 1969, NASA's Apollo 12 space vehicle artificially triggered two lightning flashes, one

1367-2630/02/000061+20$30.00

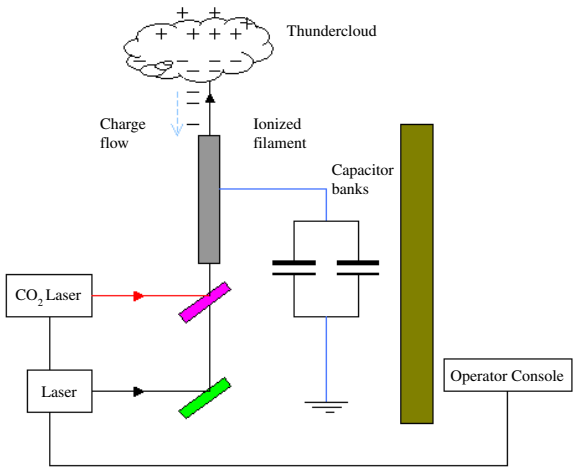

Figure 1. Proposed layout of a laser-triggered lightning energy storage.

to ground and the other an intracloud discharge, during its launch [3]. Fortunately, the vehicle survived major system upsets and the crew managed to regain control, and eventually completed their mission to the Moon successfully. With these potential dangers and threats that lightning poses, scientists have tried to devise lightning diversion techniques ranging from rocket-triggered lightning to laser-induced discharges [4]–[6].

Rocket-triggered lightning experiments, which can be seen as a modern day version of Benjamin Franklin's kite experiments, have been reported to successfully discharge electrified clouds in skies up to a success rate of 60% in New Mexico [4]. Using this technique, a rocket, tied to a large spool of wire connected to earth, was launched into the thunderclouds above. The time of launching of the rocket was determined by monitoring the electric fields underneath the thunderclouds.

Although this technique may appear feasible, it has a few setbacks. Firstly, the launching of numerous projectiles into the sky followed by their potentially dangerous downfall makes it less attractive to divert lightning from sensitive places like substations and power grids. Secondly, the rocket must be fired at very great speeds into the sky to prevent an accumulation of space charges that can effectively shield it. Thus, the rocket speed must be greater than 2×10^5 m s^{-1}, the downward speed of a stepped leader in a lightning process [7]. These shortcomings could be easily overcome with a laser-induced lightning discharge. In this technique, a collimated laser beam is used to ionize the air, thus creating a preferential conducting path for free charges in the sky to flow down to earth on a faster and more reliable basis.

It follows from the above argument that if lightning can be diverted, it may also then be possible to store these atmospheric electrical charges through the use of conducting electrodes and capacitor banks as shown in figure 1 [8]. Once the plasma filament is created through laser ionization, stray charges are collected from electrified clouds during thunderstorms or from the ionosphere in clear weather. These charges will flow through a conductive electrode as they approach the ground to avoid the possibility of artificially triggering a lightning discharge that may destroy the laser system. This electrode will then pass these charges onto a capacitor bank to store them. Utilizing this form of atmospheric electricity may provide a new alternative source of energy in the future, while discharging a thundercloud and thus reducing potential lightning strikes at sensitive airborne operation and ground installations.

2. Survey

2.1. Photoionization of air

Air is known to undergo optical breakdown at very high laser intensities, usually beyond 10^{14} W cm^{-2}. This is a direct consequence of rapid energy deposition into a small interaction or focal volume of air by the laser. Essentially, there are two main mechanisms responsible for the photoionization of air: avalanche ionization and multiphoton ionization [9].

In avalanche ionization, or sometimes known as cascade ionization, the bound electrons in the valence shell of air molecules usually have an energy bandgap greater than the incident laser photon energy. However, a small number of free electrons exist. These free electrons may be generated through high altitude ionization of air molecules, radicals, break-up of aerosol molecules, thermal ionization or multiphoton ionization. These free electrons constitute the required seed electrons for avalanche ionization. Although these free electrons may exist in small number initially and have low kinetic energy, through a process called inverse bremsstrahlung, they can be accelerated to gain enough kinetic energy to impact ionize a molecule in collision, resulting in more free but slower electrons. The whole process repeats itself with more electrons gaining higher kinetic energy, exceeding the ionization potential of the bound electrons, to impact ionize even more molecules, leading to an avalanche with the resultant formation of a plasma. In this inverse bremsstrahlung process, the free electrons absorb photons through the laser field when they collide with atoms or molecules. A free electron does not absorb laser energy directly without any collision. This is because the free electron simply quivers in the oscillating laser field, and when averaged over an optical cycle, it does not gain any net energy [10].

Based on a classical electron oscillator model, an ionization intensity threshold for avalanche ionization, I_t, can be estimated [11]:

$$I_t \propto \frac{(\omega^2 + p_{eff}^2)}{\tau_p p_{eff}} \tag{1}$$

where p_{eff} is the effective momentum transfer rate between the free electron and heavier colliding molecule and τ_p the laser pulse width of frequency ω. A closer look at this relationship will tell us that the ionization intensity threshold will be lowered if the laser pulse width is increased along with a lower laser frequency. Realizing that the effective momentum transfer rate, p_{eff}, increases with the density of neutral molecules, ρ_n, and therefore with increasing gas pressure, P, it follows that the ionization intensity threshold will be further decreased for higher gas pressures (assuming a typical case of $\omega \gg p_{eff}$). Thus, avalanche ionization will be greatly enhanced by longer laser pulse widths smaller frequencies (or longer wavelengths) and higher gas pressures.

The other dominant photoionization mechanism is the multiphoton ionization process. Through this process, bound electrons may absorb several laser photons simultaneously to overcome their ionization potential, U_I. To determine the number of photons required in an n-photon ionization of a molecule, n is simply U_I divided by $h\upsilon$ (the laser photon), rounded up to the next integer, where h is Planck's constant of 6.63×10^{-34} J s. As can be seen, multiphoton ionization depends largely on the laser operating frequency. For an ultraviolet (UV) KrF laser with a central wavelength of 248 nm, a laser photon has 5.013 eV of energy whereas a far infrared CO_2 laser with central wavelength of 10.6 μm has a photon energy of 0.1173 eV. Thus, for a nitrogen molecule with an ionization potential of 15.58 eV, the number of photons needed to ionize a nitrogen molecule is four (rounded up to the next integer) for the UV laser, or 133 for a far infrared laser.

Generation of free electrons through multiphoton ionization obeys the relationship below [12, 13]:

$$\frac{\mathrm{d}\rho_e}{\mathrm{d}t} = (\rho_0 - \rho_e)\sigma^{(n)} I(t)^n \tag{2}$$

where ρ_e is electron density, ρ_0 density of neutral molecules, $I(t)$ intensity at time t and $\sigma^{(n)}$ the n-photon ionization coefficient. When the volume of air under consideration is assumed to be unsaturated, which is typically the case, $\rho_0 \gg \rho_e$, equation (2) can be rewritten as

$$\frac{\mathrm{d}\rho_e}{\mathrm{d}t} = \rho_0 \sigma^{(n)} I(t)^n. \tag{3}$$

The solution of equation (3) has been found to be [13]

$$\rho_e = K\tau_p \rho_0 \sigma^{(n)} I_0^n \tag{4}$$

where K is the shape factor that can be calculated for any shape, I_0 is peak or initial intensity of the laser pulse, τ_p laser pulse width. For a square pulse shape, $K = 1$. The multiphoton ionization coefficient, $\sigma^{(n)}$, depends largely on the laser operating frequency with $\sigma^{(n)}$ values for UV laser pulses being very much higher than those for IR laser pulses. This dependence of $\sigma^{(n)}$ on laser frequency can be seen from the reduced number of photons needed to photoionize a neutral molecule directly for higher laser frequencies as can be seen above. $\sigma^{(n)}$ is often regarded as the effective ionization cross section of a neutral molecule. The greater its value, the greater the ionization rate. Typical values for $\sigma^{(n)}$ for n-photon ionization for molecular oxygen are 1.91×10^{-28} s^{-1} cm^6 W^{-3} (with $\lambda = 248$ nm) and 2.88×10^{-99} s^{-1} cm^{16} W^{-8} ($\lambda = 800$ nm) [14]. Furthermore, when the laser pulse width is so short that no cascade ionization of a neutral molecule can occur, multiphoton ionization dominates the photoionization process. Thus, the multiphoton ionization process will be the dominant photoionization mechanism at higher intensities (and thus shorter pulse widths), shorter wavelengths (or higher photon energies) and lower gas pressures.

2.2. *Effectiveness of shorter laser pulses*

Scientists have toyed with the idea of using power lasers to induce electrical discharges in gases and air since the 1960s [15]–[25]. The preconception back then was that the likelihood of air breakdown occurring due to the photoionization of air depended solely on the power of the laser pulse used, not its intensity. Although it was shown that powerful CO_2 infrared laser pulses could guide an electrical streamer in air up to a distance of 71 cm [26], long gap guided electrical discharges in air remained elusive. Using CO_2 gas lasers of long pulse duration, optical beads were formed along the propagation path of the laser pulse, rather than a long continuous ionized path. These beads were formed through avalanche ionization. A similar process takes place in a transparent solid material in which irreversible damage takes place when the critical density of free electrons in the material reaches 10^{18} cm^{-3} [10]. This transparent material breaks down and becomes opaque, absorbing energy from the laser field as the resultant plasma heats up. Thus, the optical plasma beads formed in air through avalanche ionization will limit the propagation distance of long pulse lasers. To penetrate these opaque beads, the laser frequency ought to be higher than that of the concomitant plasma.

To avoid this additional requirement in the laser design, a shorter laser pulse width should be used. Ultrashort laser pulses have much higher intensities compared to continuous wave and

long laser pulses. Consider a laser beam of radius 100 μm with an initial input energy of 1 mJ. A laser pulse width of 100 ms will produce a laser beam of 0.01 W power and 320 kW m^{-2} intensity. On the other hand, a laser beam of 100 fs pulse duration produces 10 GW of power with an intensity of 3.2×10^{17} W m^{-2}, 12 orders of magnitude higher than that of a 100 ms laser pulse width! Because of their high intensities, ultrashort pulse lasers are generating a wide interest in a variety of potential applications, such as laser ablation and micromachining, remote sensing and light detection and ranging (LIDAR), and laser-triggered lightning [5]–[8, 10, 11, 27, 28].

Because of the high intensities generated with ultrashort laser pulses, multiphoton ionization of air takes precedence over avalanche ionization. Here, the photoionization rate of air is controlled more easily, simply by controlling the intensity of the ultrashort laser pulses. With n being the number of photons needed to ionize a neutral molecule, the n-photon ionization rate of air is proportional to the nth power of intensity, I^n, as seen in equation (4). On the other hand, avalanche ionization may take a longer time to build up. However, once the ionization threshold is reached, the cascade or chain reaction of the free electrons may only be suppressed by lowering the air pressure, which is almost impossible in triggering outdoor electrical discharges. Also, for ultrashort pulses, the heat diffusion length is shorter [10]. Thus, air turbulence does not much affect the formation of the ionized path as the photoionization of air molecules remains in a small localized area along the beam path [29]. Table 1 shows recent experimental advances in the propagation of ultrashort laser pulses in air [27, 28, 30]–[39]. By simply utilizing femtosecond laser pulses, intense laser pulses may propagate as far as 10 km into the sky with a 6×10^{11} cm^{-3} electron density ionized path trailing the laser pulses [35]. Furthermore, the electron density values in all the aforementioned experiments exceed the minimum electron density of 5×10^{11} cm^{-3} for lightning initiation [5, 28].

2.3. Choice of laser wavelength

A comparison between ultrashort infrared (IR) and UV laser pulses in table 1 also indicates that lower input energies are needed to reach similar electron densities in the UV regime as those obtained in the IR regime. Lower input energies, in turn, translate into lower filament intensities in the UV regime (a few orders lower than that in the IR regime). This may be attributed to the much higher ionization cross-sections of the UV radiation compared to that of the infrared radiation [37]–[39]. It should be noted that in the UV regime, there is no spectral broadening or conical emission loss as reported by Schwarz *et al* [39]. Therefore, propagation losses or power attenuation should be smaller in the UV regime. The associated power loss with IR ultrashort laser pulses in the form of continuum generation is extensively investigated and exploited for LIDAR or remote sensing systems [27, 28, 35, 40]–[45].

Thus, UV laser pulses seem to be naturally the best choice for artificial initiation of lightning discharges. Since UV wavelengths are shorter, in the spectral range from 220–240 nm, they suffer less beam diffraction, hence allowing a narrower beam than a corresponding IR laser over the same propagation distance. Shorter wavelength laser pulses also have higher photon energy. This means that fewer photons are required to ionize a particular neutral molecule. Furthermore, the photoionization scenario for a UV beam will more likely be a multiphoton process, with higher multiphoton ionization coefficients. This means that, as a direct consequence of equation (2), UV laser intensities need not be very high for a given electron density produced by an IR laser pulse, as evident in table 1.

Institute of Physics DEUTSCHE PHYSIKALISCHE GESELLSCHAFT

Table 1. Recent experimental investigations into propagation of ultrashort laser pulses in air for both IR and UV regimes. (Empty space indicates an absence of reporting, and does not necessarily mean an absence of a particular phenomenon.)

	[30]	[31]	[32, 33]	[34]	[27, 28, 35]	[36]		[37, 38]		[39]	
Laser:											
Wavelength, λ (nm)	775	800	800	800	790	1053	795	248		248	800
Pulse length (fs)	200	150	∼220	120	84.93	445.9	50.96	382.2	4246	1100	200
Input energy, E_{in} (mJ)	20	30	10	5	160	10–20		2	15	0.2	2
Peak power, P (GW)	80	160	36	33	1503	20–40	150–300	4.2	2.8	0.145	8
Critical power, P_{cr} (GW)	1.7	3.4	6.1†	3.6†		3.3†	1.9†	0.122		0.098	1
n_2 (cm^2 W^{-1})	5.6×10^{-19}	3×10^{-19}	1.57×10^{-19}	2.8×10^{-19}		5×10^{-19}		8×10^{-19}		10×10^{-19}	
Filaments:											
No of filaments (max)	3	≥2	1	Several	10–20	3–4				17 m^{-1}	
Filament size (μm)	80	80–100	250	190	100	50–2000		150		100	
Propagation distance (m)	30	50	111	100	≥10 km	<100	≥200	4		12	
Energy content/ filament (mJ)	0.75	0.7–1	0.34	∼0.5		0.8		0.2			

Table 1. (Continued.)

	[30]	[31]	[32, 33]	[34]	[27, 28, 35]	[36]		[37, 38]	[39]	
Electron density (cm^{-3})		10^{16}			$\geq 6 \times 10^{11}$	10^{16}–10^{17}		10^{16}	3×10^{15}	1.5×10^{14}
Filament intensity ($W\ cm^{-2}$)	7×10^{13}	10^{14}	10^{14}	10^{14}	10^{13}			10^{11}	1.9×10^{12}	
Rayleigh range, z_R (cm)	2.6	3.9	24.5	14.2	4	1190	1580	28.5	12.5	
Observations:										
Conical emission		Yes	Yes						None	
Spectral broadening	Red-shifted	White light continuum			300–4500 nm spectrum				None	

† Based on the moving focus model, P_{cr} is taken to be $P_{cr} = (3.77\lambda^2)/(8\pi n_0 n_2)$.

3. Ultraviolet pulse model

When propagating in air, intense ultrashort laser pulses are known to self-focus due to the nonlinear optical Kerr effect. Beyond an intensity threshold, the self-focusing action of the laser beam overcomes beam diffraction, and the peak intensity of the laser beam increases. This eventually leads to photoionization and generation of a weak plasma in air. Once the plasma is formed, it defocuses the laser beam, limiting its intensity [46]. If these competing dynamics of self-focusing, diffraction and plasma defocusing are balanced, a self-guided beam scenario emerges with the laser beam propagating over many Rayleigh lengths, as demonstrated in [27]–[45]. Multiple filamentation for both IR and UV regimes has also been observed in the propagation of ultrashort laser pulses in air with peak powers several times greater than the critical power for self-focusing [30]–[39]. These light filaments may propagate as far as 100 m under laboratory conditions [32]–[34]. A number of models have been proposed in recent years to explain the highly nonlinear dynamics involved, namely the self-waveguiding, moving focus and dynamic spatial replenishment models [30]–[34, 47, 48].

In this paper, we adopt a model first proposed by Schwarz and Diels [29] and apply it to the propagation of ultrashort UV pulses in air. The UV wavelength has been chosen to be 248 nm (corresponding to a KrF laser) as the most appropriate wavelength for the triggering of electrical discharges with three-photon ionization of molecular oxygen being the dominant source of free electrons, as reported in [13, 29] and [39].

3.1. Pulse duration

To induce an electrical discharge outdoors, the laser pulse width should be long enough to create free electrons through multiphoton ionization, but short enough so that avalanche ionization does not start to kick in. Thus, the three-photon ionization rate of air at sea level is given as [5, 29]

$$\frac{\mathrm{d}\rho_e}{\mathrm{d}t} = \sigma^{(3)} I^3 \rho_n - \beta_{ep}\rho_e^2 \tag{5}$$

which is similar to equation (3), but with the inclusion of the recombination effects in air. β_{ep} is the electron–positive ion recombination coefficient and is taken to be 1.1×10^{-12} m^3 s^{-1} at sea level with corresponding measured values of $\rho_n = 5.4 \times 10^{24}$ m^{-3} and $\sigma^{(3)} = 3 \times 10^{-41}$ m^6 s^2 J^{-3} [12, 13, 39]. If we are to consider an equilibrium state, $\mathrm{d}\rho_e/\mathrm{d}t = 0$, resulting in an equilibrium electron density,

$$\rho_{eq} = \sqrt{\frac{\sigma^{(3)} I^3 \rho_n}{\beta_{ep}}} \tag{6}$$

which gives us $\rho_{eq} = 4.3 \times 10^{21}$ m^{-3} for a laser intensity of $I = 5 \times 10^{15}$ W m^{-2}. Substituting equation (6) into (5),

$$\frac{\mathrm{d}\rho}{\mathrm{d}t_N} = 1 - \rho^2 \tag{7}$$

where $\rho = \rho_e/\rho_{eq}$ and $t_N = \beta_{ep}\rho_{eq}t$ is the normalized time taken at the equilibrium density. Putting $t_N = 1$ into equation (7), calculations show that 75% of the equilibrium electron density has been reached, hence giving us the minimum time required for the pulse duration. Thus,

$$\begin{aligned} t_N &= \beta_{ep}\rho_{eq}t = 1 \\ t &= \frac{1}{\beta_{ep}\rho_{eq}}. \end{aligned} \tag{8}$$

Substituting β_{ep} and ρ_{eq} into equation (8), the minimum time required is found to be roughly 200 ps.

To find the maximum laser pulse width, we need to consider avalanche ionization. In intense laser fields, an electron gains energy, $\mathrm{d}E$, by inverse bremsstrahlung in time $\mathrm{d}t$ according to [29]

$$\frac{\mathrm{d}E}{\mathrm{d}t} = \frac{Ie^2\lambda^2 v_{ei}}{2\pi^2 c^3 \varepsilon_0 m_e} \tag{9}$$

where I is the laser intensity, e electronic charge, m_e electronic mass, c speed of light in vacuum, λ laser frequency, ε_0 electric permittivity of free space and v_{ei} the electron–ion collisional frequency, which has a value of 1.67×10^{10} s^{-1} [29]. Taking the upper limit of $\mathrm{d}E$ to be the ionization potential U_I of oxygen as 12.2 eV, we obtain the time interval Δt beyond which electron cascade ionization starts to take place in air. Δt is found to be around 63 ns.

Based on this model, a steady state analysis can be applied to the propagation of UV pulses with pulse widths ranging from 200 ps to 60 ns. This steady state analysis utilizes a standard Gaussian beam with a field amplitude [49]

$$E(r,z) = \frac{w_0}{w} E_0 \exp\left[-\frac{r^2}{w^2}\right] \exp\left[-\mathrm{i}\left(\frac{kr^2}{2R} + \phi\right)\right] \tag{10}$$

with w_0 the beam radius at e^{-2} intensity and $k = 2\pi/\lambda$ the wavenumber. The beam radius w, wavefront curvature R and phase factor ϕ are defined as follows with z being the laser propagation distance:

$$w^2(z) = w_0^2\left[1 + \left(\frac{\lambda z}{\pi w_0^2}\right)^2\right] \tag{11}$$

$$R(z) = z\left[1 + \left(\frac{\pi w_0^2}{\lambda z}\right)^2\right] \tag{12}$$

$$\phi(z) = \tan^{-1}\left(\frac{\lambda z}{\pi w_0^2}\right). \tag{13}$$

3.2. Power losses

In this UV model, as the laser beam propagates in air, it undergoes self-focusing due to the nonlinear Kerr optical effect and also defocusing through the generation of electron plasma. These effects are included in the refractive index of air as [29]

$$n = n_0 + n_2 I - n_3 I^{3/2} \tag{14}$$

where n_0 is the linear refractive index of air, $n_2 = 7.8 \times 10^{23}$ m^2 W^{-1} is the measured intensity-dependent self-focusing index and n_3 the intensity-dependent plasma defocusing refractive index

$$n_3 = \sqrt{\frac{\sigma^{(3)}\rho_n}{\beta_{ep}}}\frac{e^2}{2n_0\omega^2 m_e \varepsilon_0} \tag{15}$$

giving us $n_3 = 3.35 \times 10^{-31}$ m^2 W$^{-3/2}$ upon substitution of the above values.

Within the constraints of this model, two main mechanisms responsible for the loss in the beam power are plasma heating [50] and three-photon ionization of oxygen. These losses are accounted for in [29]

$$\frac{\mathrm{d}P}{\mathrm{d}z} = -\left(K_{MPI}\frac{1}{w^4}P^2 + K_{plasma}\frac{1}{w^3}P^{3/2}\right)P \tag{16}$$

where K_{MPI} and K_{plasma} are the three-photon power absorption and plasma nonlinear power absorption respectively given by [29]

$$K_{MPI} = \left(\frac{2}{\pi}\right)^2 (3\hbar\omega\sigma^{(3)}\rho_n) \tag{17}$$

and

$$K_{plasma} = \left(\frac{2}{\pi}\right)^{3/2} \frac{n_3}{l} \tag{18}$$

with $l = c/(2v_{ei})$ being the mean free path length of electrons in the plasma.

3.3. Beam size evolution

Starting from Maxwell's wave equation,

$$\nabla^2 \tilde{E} = \mu\varepsilon \frac{\partial^2 \tilde{E}}{\partial t^2} \tag{19}$$

the following relationship has been derived [29, 51], assuming a Gaussian beam in a cylindrical co-ordinate system.

$$\frac{\mathrm{d}^2 w}{\mathrm{d}z^2} = -\frac{4}{k^2}\left(\frac{P}{P_{cr}} - 1\right)\frac{1}{w^3} + K_{plasma}\frac{6l}{n_0}\frac{1}{w^4}P^{3/2}. \tag{20}$$

P_{cr} is an expression for the critical power for a cw laser beam:

$$P_{cr} = \frac{\lambda^2}{8\pi n_0 n_2} \tag{21}$$

$$z_R = \pi w_0^2/\lambda. \tag{22}$$

Taking $\lambda = 248$ nm and $w_0 = 100$ μm yields a critical power of 31 MW and a Rayleigh length, z_R, of 0.13 m. Beyond this critical power and in the absence of a balancing plasma defocusing term ($K_{plasma} = 0$), the laser beam self-focuses in air to a singularity at a self-focusing distance of 0.1033 m, which is slightly smaller than a Rayleigh length.

4. Simulation results and discussion

Equations (16) and (20) fully describe the spatial changes in beam size and power as the UV laser propagates in air within the constraints of this model. Computer simulation investigating various initial beam power and radius is presented and discussed here.

4.1. UV beam power and beam size variations in air

Two sets of initial conditions, namely input powers below and above the critical power P_{cr}, are chosen to study how the choice of initial beam power affects the propagation dynamics in air. Taking the initial beam power P to be 20 MW with a beam radius of $w_0 = 80$ μm, figures 2 and 3 are obtained showing the variation of beam size and power attenuation with propagation distance.

One can clearly observe in figure 2 that below the critical power for self-focusing, the laser beam diverges as it propagates in air. This divergence is simply due to linear beam diffraction. After propagating a distance of 200 m, the laser beam has a radius of 14 cm (compared to the initial size of 80 μm). Thus, below the critical power, the laser beam does not remain small and collimated.

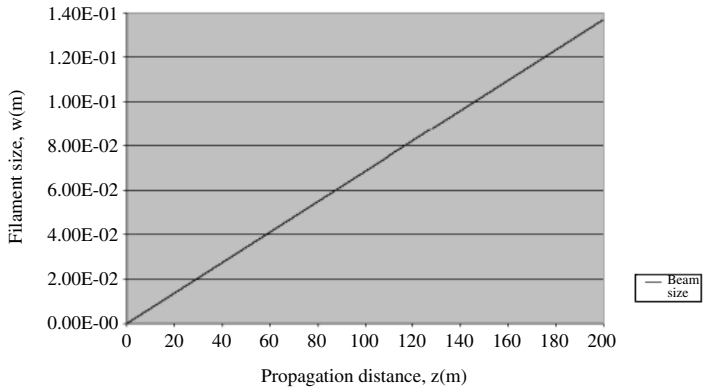

Figure 2. Beam size variation for input power (P_{in}) of 20 MW and $w_0 = 80\ \mu$m.

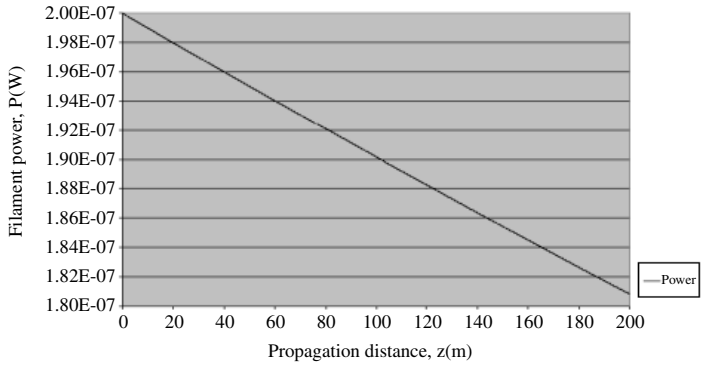

Figure 3. Power attenuation for input power (P_{in}) 20 MW and $w_0 = 80\ \mu$m.

Figure 3 indicates a linear power attenuation with propagation distance. This power loss may be attributed to the thermal blooming phenomenon associated with a high irradiance laser beam propagating in air [18]. This thermal–optical effect can be easily explained: when a high irradiance laser beam propagates through stationary air, characterized by an initial temperature T_0, density ρ_0 and index of refraction n_0, air molecules absorb the light photons, and the energy is quickly released as heat. Thus, the temperature of the air within the beam rises. The hot air near the centre of the beam axis expands radially outward (at the speed of sound). This expansion causes a decrease in the mass density, which in turn lowers the refractive index near the beam axis. The beam undergoes a weak, but nevertheless observable, defocusing similar to that which takes place when a beam is passed through a concave (negative focus) lens.

Investigations into the filamentation of UV laser pulses with initial peak powers greater than the critical power of 31 MW, but having equal initial beam size $w_0 = 80\ \mu$m, have been conducted, as shown in figures 4 and 5.

Figure 4 describes the filament size variation for different input powers ranging from 50 to 400 MW. For 50 and 100 MW input powers, the filament shows a gradual increase in the overall beam size. On the other hand, the filament experiences an initial contraction in the overall size for input powers of 200 MW and above. Furthermore, for large input powers (400 MW and beyond), the filament size tends to grow exponentially after the initial contraction. This sudden increase in the filament size is caused by the creation of a plasma channel. The initial contraction

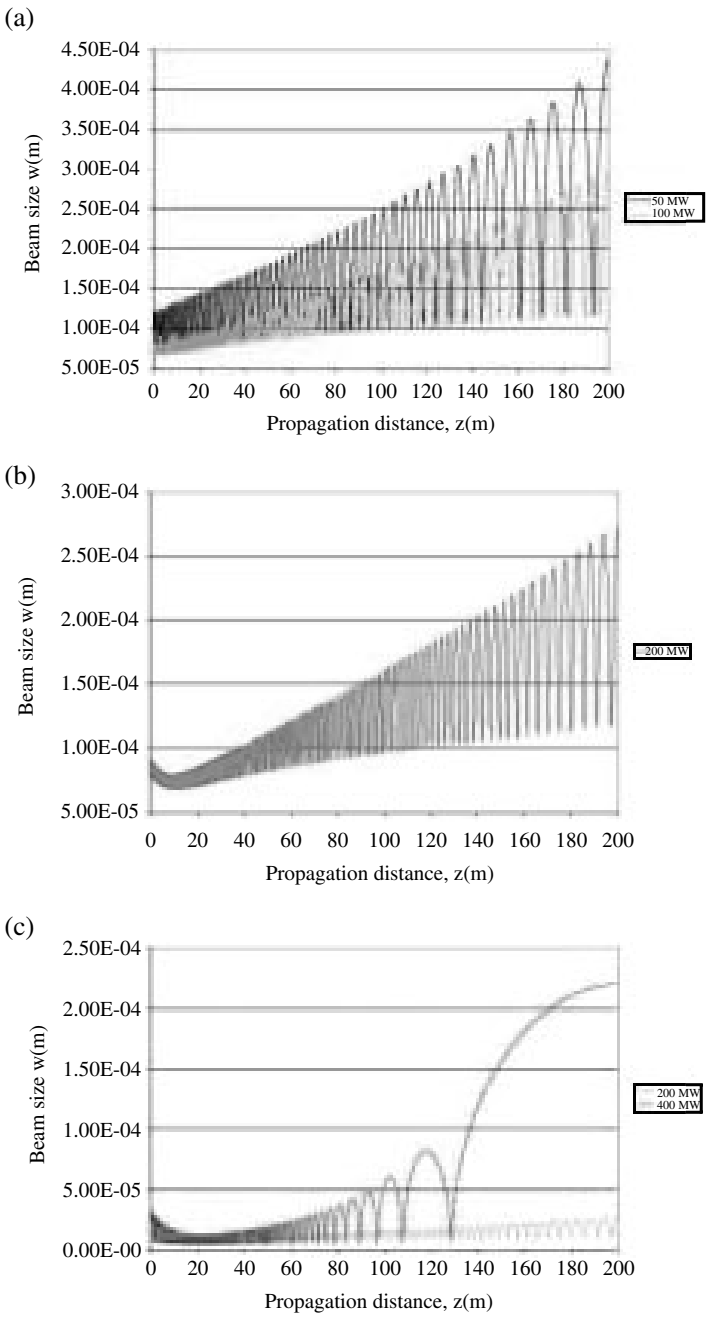

Figure 4. Beam size variation with distance for different input powers but equal $w_0 = 80\ \mu$m. (a) Beam size variation for input powers of 50 and 100 MW with $w_0 = 80\ \mu$m. (b) Beam size variation for input power 200 MW with $w_0 = 80\ \mu$m. (c) Beam size variation for input powers 200 and 400 MW with equal $w_0 = 80\ \mu$m.

in beam size results in very large intensities of the laser beam, photo-ionizing the air molecules. Once the plasma has been formed, the plasma acts to defocus the laser beam (due to the plasma defocusing refractive index n_3). The formation of plasma may be further substantiated by the marked decrease in the power transmitted through the filament in figure 4(c) for large input powers. This further reduction of power may be attributed to plasma absorption and heating.

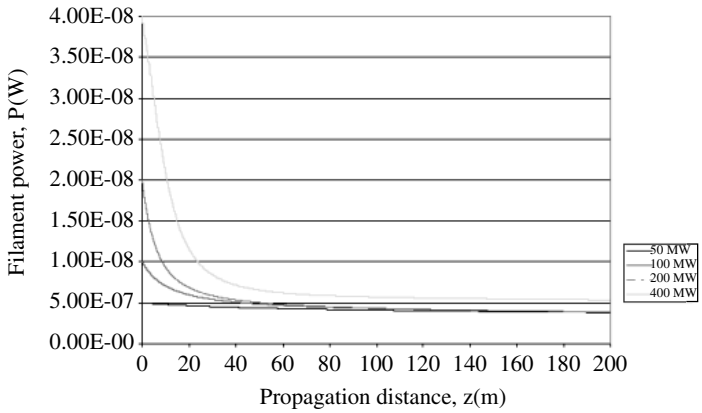

Figure 5. Power attenuation with propagation distance for input powers 50, 100, 200 and 400 MW.

From figure 5, one can see that the least percentage decrease in power transmitted in the filament occurs for the least input power, i.e. for 50 MW. As the input power increases, greater power attenuation takes place. Nevertheless, for the four different initial input powers shown above (50, 100, 200 and 400 MW), the power trapped in the filament tends to stabilize around 50 MW after propagating a distance of 100 m in all cases.

These observations are consistent with reported experimental results [30]–[39, 52]. The energy content trapped in a filament in air usually meets the required level necessary to reach the critical power P_{cr}, or being slightly higher to overcome various losses when propagating in air. These losses may be due to dispersion, Raman effects, Rayleigh losses, Brillouin scattering and plasma thermal absorption [9, 29, 47, 53]. For input powers greater than 100 MW, the drastic exponential decrease in transmitted power in the filament can be explained with the formation of multiple filaments. This phenomenon has been reported in experiments for both IR and UV regimes [9, 29, 30, 31, 35]–[39] and has also been explained theoretically [14, 28, 34, 56, 57]. Schwarz *et al* [39] have reported the formation of up to 200 UV filaments in air over a distance of 12 m with the average filament length being about 0.5 m and a generation of about 3×10^{15} cm^{-3} in electron density. These multiple filaments are also observed to interact with one another, coalescing at different lengths, giving an illusion of a continuous single filament propagating in air [47, 48, 57]–[61]. It is on this basis that the dynamic spatial replenishment model is founded. This model explains that the leading portion of an incident pulse undergoes a self-focusing collapse leading to plasma generation. Subsequently, the trailing portion of the pulse defocuses into spatial rings. Upon further propagation, the leading pulse decays due to nonlinear absorption whereas the trailing portion of the pulse reforms spatially due to self-focusing. The new emerging pulses gain energy from the outer and trailing parts of the pulse and also from new pulses, creating an illusion of a single self-waveguided pulse propagating over a long distance.

4.2. Optimal laser parameters

In deciding the best-suited parameters for long distance propagation of UV laser pulses in air, theoretical investigations have been conducted for the following conditions:

(a) Different beam sizes with the same input power.

(b) Different input powers of the same initial beam size.

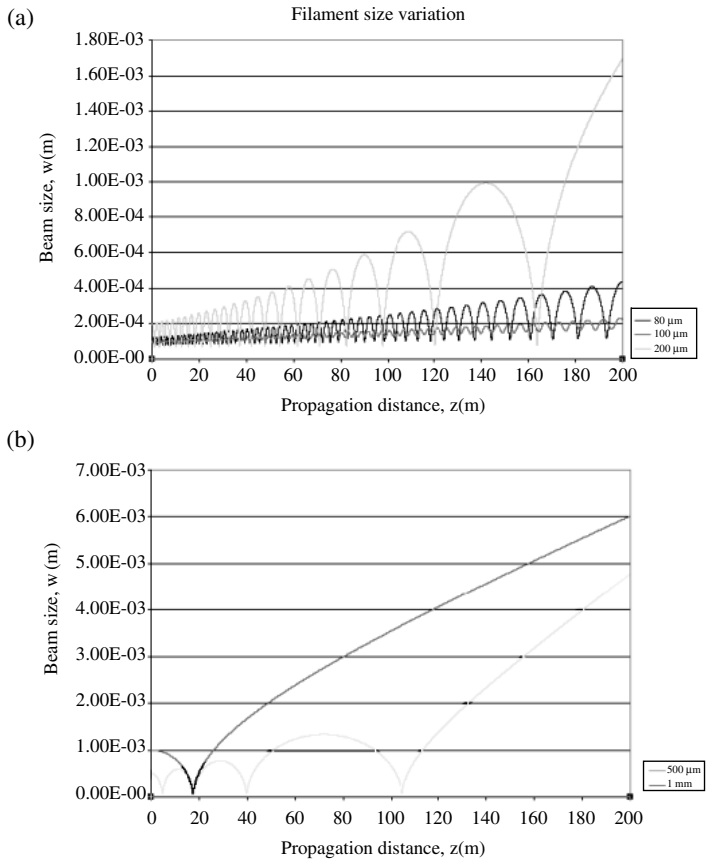

Figure 6. Filament size variation for w_0 values of 80, 100, 200, 500 and 1000 μm for $P = 50$ MW.

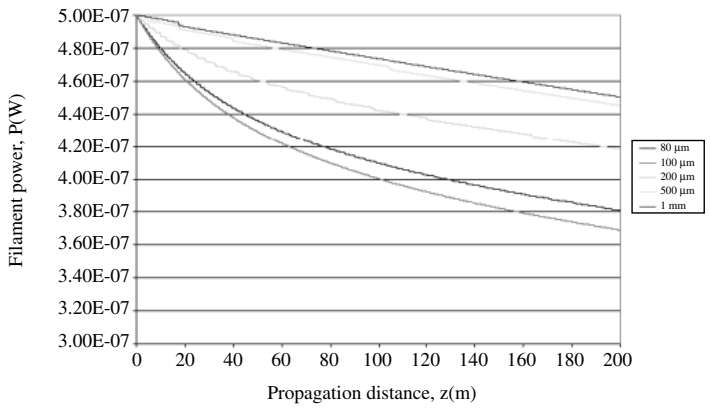

Figure 7. Power attenuation with $P = 50$ MW for different w_0.

4.2.1. Choice of laser beam size. Setting the input power P to be constant at 50 MW for various beam sizes w of 80, 100, 200 and 400 μm, figures 6 and 7 were obtained.

Based on figure 6, $w_0 = 100$ μm appears to be the best choice for an initial beam size parameter. For this value, the beam size remains the smallest (and thus higher laser intensity trapped in the filament) after a propagation distance of 200 m. Figure 7 further consolidates this

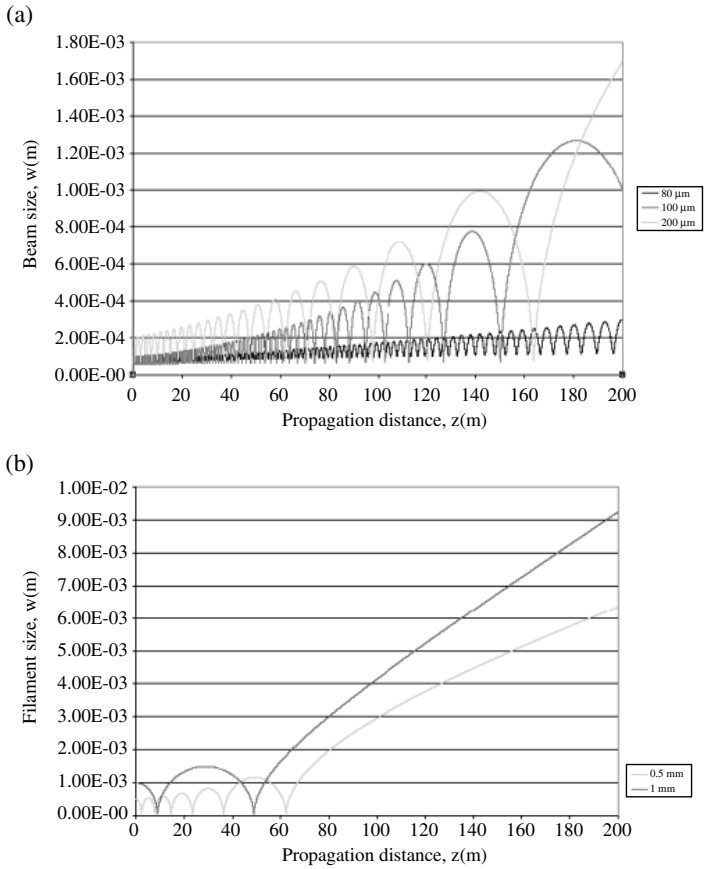

Figure 8. Filament size variation for different w_0 of 80, 100, 200, 500 and 1000 μm with $P = 100$ MW.

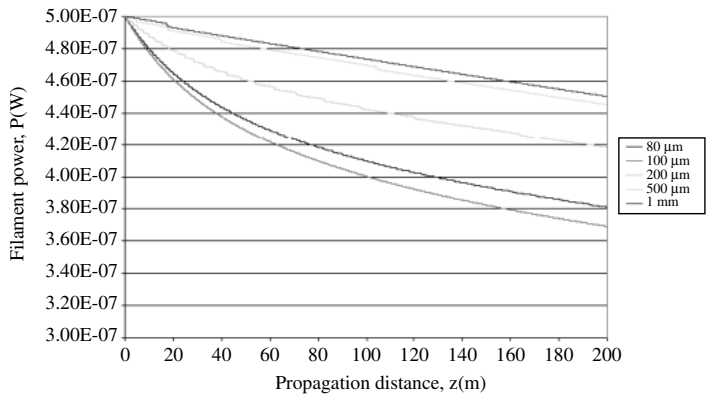

Figure 9. Power attenuation with $P = 100$ MW for different w_0.

choice. Although the power attenuation factor is largest when $w_0 = 100$ μm, the laser intensity in the beam is the highest (roughly 4.8×10^{14} W m^{-2}) compared to $w_0 = 1000$ μm (lowest power attenuation factor) with an intensity of 8×10^{14} W m^{-2}. It is important to remember that laser intensity (rather than the input power) plays a very important role in the multiphoton ionization process, generating free electrons that will facilitate the initiation of a lightning discharge, as

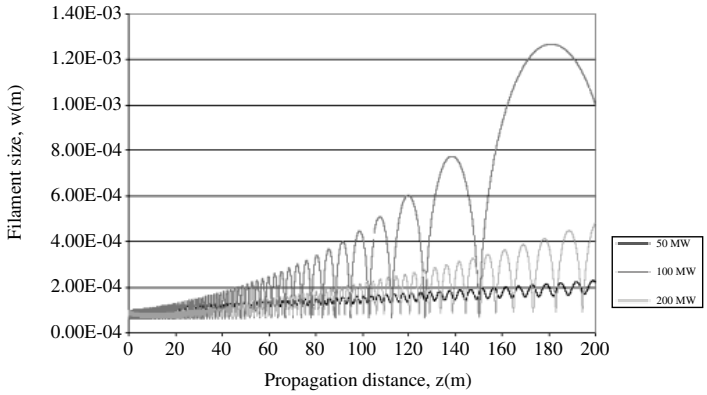

Figure 10. Beam size variation for different input powers but with constant $w_0 = 100\ \mu$m.

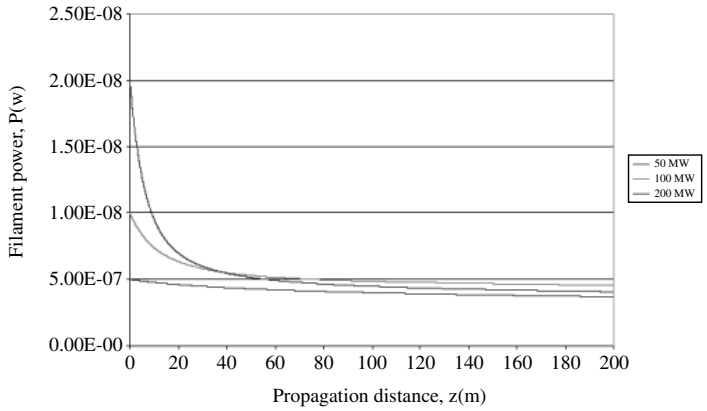

Figure 11. Power attenuation for different input powers with $w_0 = 100\ \mu$m.

supported by equation (2). The laser intensities associated with the remaining beam sizes 80, 200 and 500 μm are roughly 2.69×10^{14}, 9.2×10^{12} and 1.3×10^{12} W m^{-2} respectively.

However, when the input power was set at a constant 100 MW, 80 μm appears to be the best initial beam size (figures 8 and 9) with an intensity of about 2.7×10^{14} W m^{-2}. This intensity is still lower than that achieved with a laser beam size of 100 μm and input power of 50 MW although the energy requirement on the laser has now been doubled. Thus, a 50 MW UV laser pulse with a beam size of 100 μm is still the preferred choice.

4.2.2. Choice of beam input power. Different input powers (50, 100 and 200 MW) with a (constant) initial beam size $w_0 = 100\ \mu$m were used to test the validity of using a 100 μm beam size. The results are shown in figures 10 and 11.

Figure 10 displays a minimal beam size variation when $P = 50$ MW was used. After a propagation distance of 200 m, the beam size remains smaller than 0.3 mm in radius. One may also expect a large beam size modulational instability for input powers greater than 200 MW. In figure 11, the 50 MW input power filament also shows the least power attenuation factor while maintaining the largest beam intensity after propagating more than 200 m in air.

5. Conclusion

Through the simulation work and within the limits of the model presented above, it is concluded that UV (with a central wavelength of 248 nm) laser pulses with pulse width of 200 ps, peak power 50 MW and a beam size of 100 μm are seen as the optimal tool to initiate outdoor lightning. The input energy requirement for such a laser system is 12.5 mJ given by [14]

$$E_{in} = P_{in} \times \tau_p \sqrt{\frac{\pi}{2}} \tag{23}$$

where E_{in} is the input energy, P_{in} is the initial peak power and τ_P is the pulse width.

One may increase the peak power of a laser pulse by decreasing the pulse duration (or the pulse width) while maintaining the same input energy. For this reason, the input energy of a laser beam is vital only for determining the peak power of a laser pulse. As long as the laser peak power remains larger than the critical power, P_{cr}, defined in equation (21), self-filamentation of UV pulses takes place.

It is also evident from the simulation that the laser beam size remains small (less than 0.3 mm in radius) even after propagating a distance of 200 m in air. These optimized laser beam parameters produce the least power attenuation of the beam and also the least variation on the overall beam size (as compared with those associated with higher initial peak powers and bigger initial beam radii).

With high peak powers (larger than 100 MW), the power trapped in the UV filaments undergoes a drastic decay for the first 30 m before finally reaching a lower power threshold of 50–60 MW. The overall filament size, at first, decreases to a minimum at a distance of 20–30 m. Beyond this point, the beam size increases almost exponentially (for the higher peak powers). Consequently, there is also a concomitant reduction in laser intensity in the filament. This decrease in the filament power and intensities may hinder the photoionization process of air molecules at long distances. Nonetheless, it may be postulated that this sudden drop in power can be attributed to the formation of multiple filaments in the path of the propagating laser pulses [52].

Acknowledgments

We kindly acknowledge the assistance of Professor J C Diels and Dr J Schwarz of University of New Mexico, USA. This study has been made possible through their guidance and insights into the physics of the highly nonlinear phenomenon of ultrashort pulse lasers propagating in air.

References

[1] Kithil R 2002 National Lightning Safety Institute (NLSI) *Lightning Accidents and Incidents* webpage http://www.lightningsafety.com/nlsi_lls.html (accessed on 2 April 2002)

[2] Wired Digital Inc. 1999 *Groaning Grids* webpage http://www.wired.com/wired/archive/7.04/grids.html (accessed on 2 April 2002)

[3] Goodman S 2002 *A Lightning Primer* webpage http://thunder.msfc.nasa.gov/primer/index.html (accessed on 2 April 2002)

[4] Hubert P and Laroche P 1984 Triggered lightning in New Mexico *J. Geophys. Res.* **89** D2 2511–21

[5] Xin M Z, Diels J C, Cai Y W and Elizondo J M 1995 Femtosecond ultraviolet laser pulse induced lightning discharges in gases *IEEE J. Quantum Electron.* **31** 599–612

[6] La Fontaine B, Vidal F, Comtois D, Chien C Y, Desparois A, Johnston T W, Kieffer J C, Hubert P M, Pepin H and Rizk F A M 1999 The influence of electron density on the formation of streamers in electrical discharges triggered with ultrashort laser pulses *IEEE Trans. Plasma Sci.* **27** 688–700
[7] Martin A and Uman 1994 Natural lightning *IEEE Trans. Ind. Appl.* **30** 785–90
[8] Khan N, Mariun N and Yeak J 2000 Prospects of atmospheric electricity in Malaysia *IEEE TENCON Conf. Proc.* vol 3 pp 200–6
[9] Shen Y R 1991 *The Principles of Nonlinear Optics* (Singapore: Wiley)
[10] Liu X, Du D and Mourou G 1997 Laser ablation and micromachining with ultrashort laser pulses *IEEE J. Quantum Electron.* **33** 1706–16
[11] Rambo P 2000 Laser-induced lightning *PhD Thesis* University of New Mexico
[12] Rambo P, Schwarz J and Diels J C 2001 High-voltage electrical discharges induced by an ultrashort-pulse UV laser system *J. Opt. A: Pure Appl. Opt.* **3** 146–58
[13] Schwarz J, Rambo P and Diels J C 2001 Measurements of multiphoton ionization coefficients with ultrashort laser pulses *Appl. Phys.* B **72** 343–7
[14] Couairon A and Berge L 2002 Light filaments in air for ultraviolet and infrared wavelengths *Phys. Rev. Lett.* **88** 135003
[15] Gili D H and Dougal A A 1965 Breakdown minima due to electron-impact ionization in super-high-pressure gases irradiated by a focused giant-pulse laser *Phys. Rev. Lett.* **15** 845–7
[16] Buscher H T, Tomlinson R G and Damon E K 1965 Frequency dependence of optically induced breakdown *Phys. Rev. Lett.* **15** 847–9
[17] Alcock A J and Richardson M C 1968 Creation of spark by a single subnanosecond laser pulse *Phys. Rev. Lett.* **21** 667–70
[18] Kleiman H and O'Neil R W 1973 Thermal blooming of pulsed laser radiation *Appl. Phys. Lett.* **23** 43–4
[19] Denes L J and Lowke J J 1973 V–I characteristics of pulsed CO_2 laser discharges *Appl. Phys. Lett.* **23** 130–2
[20] Hacker M P, Cohn D R and Lax B 1973 Low-pressure gas breakdown with CO_2 laser radiation *Appl. Phys. Lett.* **23** 392–4
[21] Ireland C L M and Morgan C G 1973 Gas breakdown by a short laser pulse *J. Phys. D: Appl. Phys.* **6** 720–9
[22] Lencioni D E 1973 The effect of dust on 10.6 μm laser-induced air breakdown *Appl. Phys. Lett.* **23** 12–14
[23] Ireland C L M and Morgan C G 1974 Gas breakdown by single $\sim$20 ps, 1.06 and 0.53 μm laser pulses *J. Phys. D: Appl. Phys.* **7** L87–90
[24] Tulip J and Seguin H 1973 Influence of a transverse electric field on laser-induced gas breakdown *Appl. Phys. Lett.* **23** 135–6
[25] Yablonovitch E 1973 Similarity principles for laser-induced breakdown in gases *Appl. Phys. Lett.* **23** 121–2
[26] Koopman D W and Wilkerson T D 1971 Channeling of an ionizing electrical streamer by a laser beam *J. Appl. Phys.* **42** 1883–6
[27] Rairoux P, Schillinger H, Niedermeier S, Rodriguez M, Ronneberger F, Sauerbrey R, Stein B, Waite D, Wedekind C, Wille H, Woste H and Ziener C 2000 Remote sensing of the atmosphere using ultrashort laser pulses *Appl. Phys.* B **71** 573–80
[28] Schillinger H and Sauerbrey R 1999 Electrical conductivity of long plasma channels in air generated by self-guided femtosecond laser pulses *Appl. Phys.* B **68** 753–6
[29] Schwarz J and Diels J C 2001.Analytical solution for UV filaments *Phys. Rev.* A **65** 013806
[30] Braun A, Korn G, Liu X, Du D, Squier J and Mourou G 1997 Self-channeling of high-peak-power femtosecond laser pulses in air *Opt. Lett.* **20** 73–5
[31] Nibbering E T J, Curley P F, Prade B S, Franco M A, Salin F and Mysyrowicz A 1996 Conical emission from self-guided femtosecond pulses in air *Opt. Lett.* **21** 62–4
[32] Brodeur, Chien C Y, Ilkov F A and Chin S L 1997 Moving focus in the propagation of ultrashort laser pulses in air *Opt. Lett.* **22** 304–6
[33] Kosareva O G, Kandidov V P, Brodeur A, Chien C Y and Chin S L 1997 Conical emission from laser-plasma interactions in the filamentation of powerful ultrashort laser pulses in air *Opt. Lett.* **22** 1332–4
[34] Lange H R, Grillon G, Ripoche J-F, Franco M A, Lamouroux B, Prade B S, Mysyrowicz A, Nibbering E T J

and Chiron A 1998 Anomalous long-range propagation of femtosecond laser pulses through air: moving focus or pulse self-guiding? *Opt. Lett.* **23** 120–2

[35] Sauerbrey R, Niedermeier S, Franco M, Kasparian J, Mondelain D, Mysyrowicz A, Prade B, Rairoux P, Rodriguez M, Ronneberger F, Schillinger H, Tzortzakis S, Wille H, Wolf J P, Woste L and Yu J 2000 Long range propagation of terawatt laser pulses in the earth's atmosphere *QELS 2000: Quantum Electronics and Laser Science Conf. 2000, Technical Digest* vol 200 pp 142–3

[36] La Fontaine B, Vidal F, Jiang Z, Chien C Y, Comtois D, Desparois A, Johnston T W, Kieffer J C, Pepin H and Mercure H P 1999 Filamentation of ultrashort pulse laser beams resulting from their propagation over long distances in air *Phys. Plasmas* **6** 1615–21

[37] Tzortzakis S, Lamouroux B, Chiron A, Franco M, Prade B, Mysyrowicz A and Moustaizis S D 2000 Nonlinear propagation of subpicosecond ultraviolet laser pulses in air *Opt. Lett.* **25** 1270–2

[38] Tzortzakis S, Lamouroux B, Chiron A, Moustaizis S D, Anglos D, Franco M, Prade B and Mysyrowicz A 2001 Femtosecond and picosecond ultraviolet laser filaments in air: experiments and simulations *Opt. Commun.* **197** 131–43

[39] Schwarz J, Rambo P, Diels J C, Kolesik M, Wright E M and Moloney J V 2000 Ultraviolet filamentation in air *Opt. Commun.* **180** 383–90

[40] Nishioka H, Odajima W, Ueda K and Takuma H 1995 Ultrabroadband flat continuum generation in multichannel propagation of terrawatt Ti:sapphire laser pulses *Opt. Lett.* **20** 2505–7

[41] Sekikawa T, Kumazaki T, Kobayashi Y, Nabekawa Y and Watanabe S 1998 Femtosecond extreme-ultraviolet quasi-continuum generation by an intense femtosecond Ti:sapphire laser *J. Opt. Soc. Am.* B **15** 1406–9

[42] Brodeur A and Chin S L 1999 Ultrafast white-light continuum generation and self-focusing in transparent media *J. Opt. Soc. Am.* B **16** 637–50

[43] Gaeta A L 2000 Catastrophic collapse of ultrashort pulses *Phys. Rev. Lett.* **84** 3582–5

[44] Yu J, Mondelain D, Ange G, Volk R, Niedermeier S, Wolf J P, Kasparian J and Sauerbrey R 2001 Backward supercontinuum emission from a filament generated by ultrashort laser pulses in air *Opt. Lett.* **26** 533–5

[45] Kasparian J, Sauerbrey R, Mondelain D, Niedermeier S, Yu J, Wolf J P, Andre Y B, Franco M, Prade B, Tzortzakis S, Mysyrowicz A, Rodriguez M, Wille H and Woste L 2000 Infrared extension of the supercontinuum generated by femtosecond terawatt laser pulses propagating in the atmosphere *Opt. Lett.* **25** 1397–9

[46] Esarey E, Sprangle P, Krall J and Ting A 1997 Self-focusing and guiding of short laser pulses in ionizing gases and plasmas *IEEE J. Quantum Electron.* **33** 1879–914

[47] Mlejnek M, Wright E M and Moloney J V 1998 Dynamic spatial replenishment of femtosecond pulses propagating in air *Opt. Lett.* **23** 382–4

[48] Mlejnek E M, Wright E M and Moloney J V 1999 Moving-focus versus self-waveguiding model for long-distance propagation of femtosecond pulses in air *IEEE J. Quantum Electron.* **35** 1771–6

[49] Svelto O 1998 Ray and wave propagation *Principles of Lasers* 4th edn (London: Plenum) pp 127–60

[50] Jackson J D 1998 *Classical Electrodynamics* 3rd edn (New York: Wiley)

[51] Yeak J 2001 Parametric optimization of laser-triggered lightning *Masters Thesis* Universiti Putra Malaysia

[52] La Fontaine B, Comtois D, Chien C Y, Desparois A, Genin F, Jarry G, Johnston T W, Kieffer J C, Martin F, Mawassi R, Pepin H, Rizk F A M, Vidal F, Potvin C, Couture P and Mercure H P 2000 Guiding large-spark discharges with ultrashort pulse laser filaments *J. Appl. Phys.* **88** 610–15

[53] Mori W B 1997 The physics of the nonlinear optics of plasmas at relativistic intensities for short-pulse lasers *IEEE J. Quantum Electron.* **33** 1942–53

[54] Cheng C C, Wright E M and Moloney J V 2001 Generation of electromagnetic pulses from plasma channels induced by femtosecond light strings *Phys. Rev. Lett.* **87** 213001–4

[55] Tzortzakis S, Berge L, Couairon A, Franco M, Prade B and Mysyrowicz A 2001 Breakup and fusion of self-guided femtosecond light pulses in air *Phys. Rev. Lett.* **86** 5470–3

[56] Schjodt-Eriksen J, Moloney J V, Wright E M, Feng Q and Christiansen P L 2001 Polarization instability of femtosecond pulse splitting in normally dispersive self-focusing media *Opt. Lett.* **26** 78–80

[57] Akozbek N, Scalora M, Bowden C M and Chin S L 2001 White-light generation and filamentation during the propagation of ultra-short laser pulses in air *Opt. Commun.* **191** 353–62
[58] Mlejnek M, Kolesik M, Moloney J V and Wright E M 1999 Optically turbulent femtosecond light guide in air *Phys. Rev. Lett.* **83** 2938–41
[59] Talebpour A, Petit S and Chin S L 1999 Re-focusing during the propagation of a focused femtosecond Ti:sapphire laser pulse in air *Opt. Commun.* **171** 285–90
[60] Zozulya A A and Diddams S A 1999 Dynamics of self-focused femtosecond laser pulses in the near and far fields *Opt. Express* **4** 336–43
[61] Mlejnek M, Wright E M and Moloney J V 1999 *Opt. Express* **4** 223–8